ELSEVIER

Journal of Nuclear Materials 257 (1998) 318–330

journal of nuclear materials

An analysis of density distribution in UO_2 green pellet by finite element method

K. Yanai [a,*], M. Hirai [a], T. Ishikawa [b], J. Ishizaki [b], H. Saitoh [c]

[a] *Nippon Nuclear Fuel Development Co., Ltd., 2163, Narita-cho, Oarai-machi, Higashi-ibaraki-gun, Ibaraki-ken 311-13, Japan*
[b] *Japan Nuclear Fuel Co., Ltd., 3-1, 2-chome Uchikawa, Yokosuka-shi, Kanagawa-ken 239, Japan*
[c] *CRC Research Institute, Inc., 2-7-5, Minamisuna, Koto-ku, Tokyo 136, Japan*

Received 23 June 1997; accepted 16 May 1998

Abstract

A code for analyzing density distribution in UO_2 green pellet was developed using a finite element method. Calculated results using this code were compared with measured local densities in the UO_2 green pellet determined by Energy dispersive X-ray analysis (EDX). According to code analyses, axial density fluctuation along the lateral surface of the green pellet increases with the increase of the length to diameter ratio of the green pellet

Nomenclature

ϵ	total strain
ϵ_e	elastic strain
ϵ_p	plastic strain
ϵ_{ij}^e	elastic component of strain tensor
σ_m	mean normal stress
ν	Poisson's ratio
E	Young's modulus
E'	effective elastic constant
δ_{ij}	Kronecker's delta
s_{ij}	deviatric stress tensor
σ_z	axial stress
ϵ_z^e	axial elastic strain
$\sigma_z, \sigma_r, \sigma_\theta$	normal stresses
$\tau_{zr}, \tau_r\theta, \tau_\theta z$	shear stress
ξ	radial stress to axial stress ratio ($\xi = \sigma_r/\sigma_z$)
σ_{eq}, A, m, n	material constants of UO_2 power
ρ	relative density of UO_2 green pellet normalized by the theoretical density of UO_2
ρ_b	relative density of UO_2 powder bed normalized by the theoretical density of UO_2
σ_f	friction force between die surface and UO_2 powder during double acting dry press process
μ	friction coefficient between die surface and UO_2 powder during double acting dry press process
σ_r	radial stress during double acting dry press process

1. Introduction

Cylindrical UO_2 fuel pellets are fabricated from UO_2 powder which is the starting material for the pelletizing route. UO_2 powder is usually compacted under a dry condition to form a cylindrical green pellet prior to sintering. The properties of the green pellet strongly affect the properties of the sintered pellet; for example, a defect in the green pellet at its corner portion is considered to lead to endcapping of sintered pellet which is undesirable for getting a high fabrication yield. Those defects in the green pellet are attributed to heterogeneous stress distribution during or after the compaction process [1,2]. Density fluctuation in the green pellet

* Corresponding author. Tel.: +81-29 266 2131; fax: +81-29 266 2589.

0022-3115/98/$ – see front matter
PII: S0022-3115(98)00438-3

results in deformation of the sintered pellet because of density homogenization during the sintering process [3]. In the double acting dry press process of UO_2 powder, the shape of the pellet deforms during sintering from a cylindrical shape to an hourglass-like shape having a thinner diameter at its center portion along the axial direction; the behavior is called hourglassing. But, the diametral fluctuation of the UO_2 pellet, even in the case of less than one percent of the diameter, affects various performance of the pellet in the reactor, for example, pellet cladding interaction (PCI) [4]. In order to improve the reliability of the fuel performance in the reactor, the UO_2 pellets are usually ground after sintering to meet the diametral specification. Hence, this deformation of the sintered pellet should be decreased in order to minimize grinding loss of UO_2 which would raise the pellet fabrication cost, and it is very important to evaluate the density distribution in the UO_2 green pellet to control the quantity of centerless grinding of the sintered pellet.

In order to study the above characteristics, there are several measurement techniques for local density in the green pellet [5–8]. All of them are destructive techniques and much time consuming. Using them, it is hard to evaluate the compaction behavior of UO_2 powder under the double acting dry press process which has many kinds of parameters, such as compaction pressure, pellet length to diameter ratio, or chamfer shape. Then, a simulation tool for the compaction process is needed to improve compaction conditions of UO_2 powder.

There have been a number of studies involving simulations of powder particle motion by the distinct element method (DEM) [9], or finite element method (FEM) [10–12] in which the powder is assumed to be a continuum. With DEM, various motions of powder particles have been analyzed, for example, particle flow from a hopper [13], compaction [14–17], or particle segregation under vibration [18]. In their analyses by DEM, powder particles were assumed to have simple shape, namely, sphere or circular disk so as to avoid requirements of a very large memory and CPU time for the analysis in the case of irregular shaped particles. The number of powder particles is restricted by the calculation time. For both cases of wet and dry fabrication routes of UO_2 powder, UO_2 powder particles usually have distorted shapes and diameter smaller than 1 μm and are partially aggregated during powder fabrication process including heat treatment, milling and slugging. From the above limitations for the analysis by DEM and characteristics of UO_2 powder particle, DEM is considered to be inappropriate for quantitative analysis of the compaction behavior of UO_2 powder.

On the other hand, there are no such limitations in the analysis for a continuum by FEM. In the present study, FEM was applied to quantitative analysis of stresses and density distribution in UO_2 green pellet during the double acting dry press process. In order to analyze the compaction behavior of UO_2 powder by FEM, the UO_2 powder was assumed to be a continuum of an elastic-plastic material.

2. Analysis aspects by FEM

The cylindrical UO_2 green pellet is usually fabricated in a double acting dry press (Fig. 1). The procedure can be treated as an axi-symmetric problem. FEM analysis is performed for the first quadrant (half height) of an axial cross section of the cylindrical UO_2 green pellet. In this analysis, an isoparametric quadrilateral element having eight nodal points with a bilinear shape function was

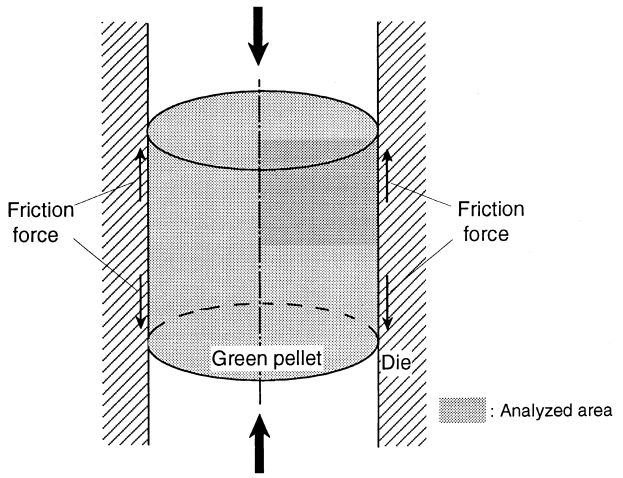

Fig. 1. Double acting dry press of UO_2 powder.

used. The initial positions of nodal points can be set freely in both radial and axial directions in this code. Strains or stresses in these elements were calculated at four Gauss points in each element. The strain-displacement correlation (strain shape function: B-matrix) was renewed at each calculation step to express the large deformation of green pellet during powder compaction (Fig. 2). For solution of a non-linear problem, the Newton–Raphson method [19] was applied.

For improving the accuracy of the calculation results of local densities in the green pellet, the local densities calculated at each step were corrected by the calculation procedure represented in Fig. 3.

The boundary conditions for this calculation are summarized in Fig. 4. There are three assumptions in this analysis.

1. Die and punch wall contacting with the UO_2 powder are rigid and cannot be deformed. (Diameter of the green pellet is constant during compaction.)
2. Friction coefficient between the die surface and UO_2 powder is constant during compaction.
3. The green pellet continues to contact with the upper and lower punches during all of the compaction process.

This FEM code is named EPOCH (Evaluation tool for POwder Compaction beHavior).

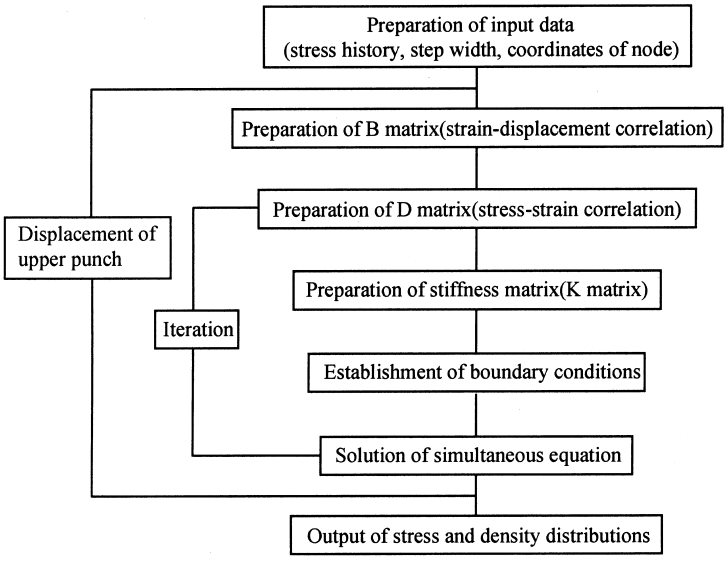

Fig. 2. Flowsheet of FEM calculation in EPOCH code.

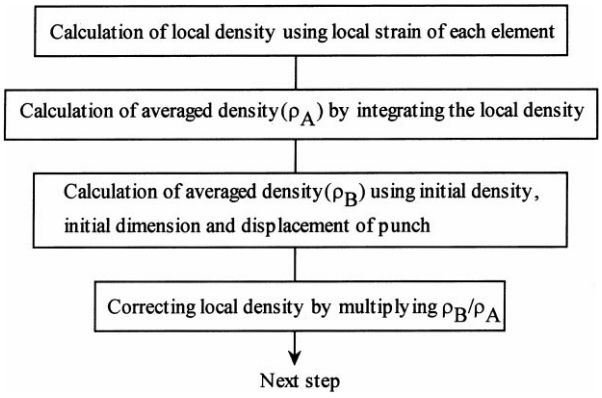

Fig. 3. Correction procedure of green density in EPOCH code.

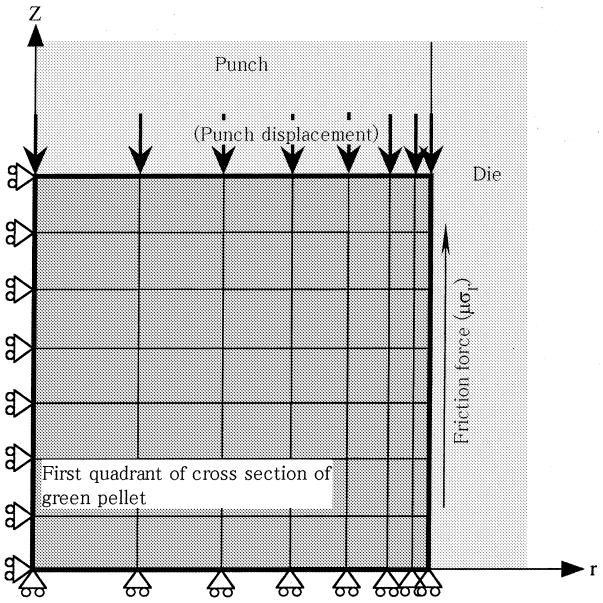

Fig. 4. Boundary condition of FEM analysis of double acting dry press of UO_2 powder.

3. Description of material properties of UO_2 powder

In the present study, UO_2 powder fabricated by the ammonium diuranate (ADU) fabrication route was used for description of deformation behavior to be implemented in the FEM code. This powder has many aggregates which cannot be evaluated easily as to whether they are destroyed during powder compaction, and it has very distorted shapes of primary and aggregate particles (Fig. 5).

Typically, apparent density of the UO_2 powder bed increases during the dry compaction process from 0.1–0.2 to 0.5–0.6 (relative density normalized by the theoretical density of UO_2). Although hardly any plastic deformation of primary powder particles occurs in this process, the apparent density changes by rearrangement of powder particles which leads to decreasing pore volume between powder particles. This macroscopic deformation of the UO_2 powder bed is similar to the plastic deformation of a porous continuum. The powder bed after compaction (green pellet) shows elastic expansion in the depressing process, which is called springback.

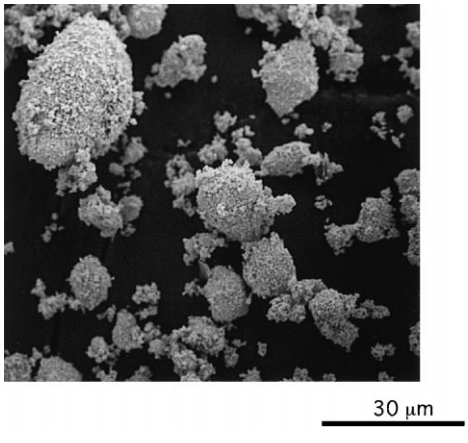

Fig. 5. UO_2 powder fabricated from ADU route.

According to these behaviors of UO_2 powder, UO_2 powder was assumed to be a porous continuum, and an elastic-plastic model was applied to analyze its compaction behavior. The total strain rate of UO_2 powder was expressed by the following equation:

$$d\varepsilon/dt = d\varepsilon_e/dt + d\varepsilon_p/dt, \quad (1)$$

where ε is the total strain, ε_e is the elastic strain and ε_p is the plastic strain of UO_2 powder bed.

For expression of elastic deformation of UO_2 powder, an isotropic elastic model for equivalent elastic material was applied. This model was expressed by the following equation:

$$d\varepsilon_{ij}^e = (1-2v)/E d\sigma m\delta ij + (1+v)/E\, ds_{ij}, \quad (2)$$

where $\varepsilon_{ij}{}^e$ is elastic component of strain tensor, v is the Poisson's ratio, E is the Young's Modulus, σ_m is the mean normal stress, δ_{ij} is the Kronecker's delta, and s_{ij} is the deviatric stress tensor.

Based on an experiment using the cylindrical double acting dry press, the effective elastic constant of the UO_2 powder can be expressed by the following equation:

$$E' = (1 - v)\sigma z/\epsilon_z^e. \quad (3)$$

In this study, this effective elastic constant was used as Young's Modulus of the UO_2 powder. Using measured data of elastic strain during the depressing process of the double acting press (ϵ_z^e) in the compaction pressure (σ_z) range of 50–400 MPa and the Poisson's ratio of Al_2O_3 ($=0.32$ [20]), the effective elastic constant of the UO_2 powder is expressed in Fig. 6. From this figure, the effective elastic constant of the UO_2 powder bed increases with its apparent density toward the value of the Young's modulus of sintered UO_2 ($\sim$200 GPa) [21]. This result shows that the UO_2 powder bed is hardened as its apparent density increases exponentially. The effective elastic constant of UO_2 powder was formulated as a function of apparent density of UO_2 powder:

$$E' = k_1(1 - v)10^{k_2(\rho - \rho b)}, \quad (4)$$

where ρ is relative density of UO_2 green pellet normalized by the theoretical density of UO_2, ρ_b is apparent density of UO_2 powder bed under a no compressive condition and k_1, k_2 are material constants of UO_2 powder.

In order to express the plastic behavior of UO_2 powder, the yield function for porous metals developed by Shima and Oyane [22] was applied in this study. According to their theory, the yield function was expressed by the following equations:

$$(f_2\sigma_{eq})^2 = ((\sigma_z - \sigma_r)^2 + (\sigma_r - \sigma_\theta)^2 + (\sigma_\theta - \sigma_z)^2 + 6(\tau_{zr^2} + \tau_{r\theta^2} + \tau_{\theta z^2}))/2 + (f_1\sigma_m)^2, \quad (5)$$

$$f_1 = A(1 - \rho)^m = ((9(1 - \xi))/(2(1 + 2\xi)))^{0.5}, \quad (6)$$

$$f_2 = \rho^n = (3(1 - \xi)/2)^{0.5}\sigma_z, \quad (7)$$

where σ_z, σ_r, σ_θ are normal stresses, τ_{zr}, $\tau_{r\theta}$, $\tau_{\theta z}$ are shear stresses, σ_m is mean normal stress, ξ is radial stress to axial stress ratio ($\xi = \sigma_r/\sigma_z$), and σ_{eq}, A, m, n are material constants which must be determined by experiments. This yield function, described as a function of apparent density of porous material, can express the deformation behavior change of powdered material due to the increase of the apparent density during the double acting dry press process.

The radial stress to axial stress ratio (ξ) during compaction_was measured using a die divided into two parts [23] and the results are shown in Fig. 7. ξ increases with green density. In this study, ξ was expressed by

$$\xi = a - b/(\rho - \rho_b + b/a), \quad (8)$$

where a and b are material constants which were determined by best fitting to experimental data.

Figs. 8 and 9 show f_1 and f_2 which were calculated by Eqs. (6) and (7) [23] using ξ data and the relationship between stress and green density of UO_2 (Fig. 10). From the slopes and intercepts of the ordinates by the fitting lines in Figs. 8 and 9, material constants of σ_{eq}, A, m, n were calculated. Table 1 summarizes material constants of the UO_2 powder.

4. Friction coefficient between UO_2 powder and die surface

The friction force between the die surface and UO_2 powder can be expressed using the friction coefficient as follows:

$$\sigma_f = \mu\sigma_r = \mu\xi\sigma_z, \quad (9)$$

$$\mu = (\sigma_f/\sigma_z)/\xi, \quad (10)$$

where σ_f is friction force between the die surface and UO_2 powder, μ is friction coefficient, and σ_r is radial stress at the lateral surface of UO_2 green pellet. The

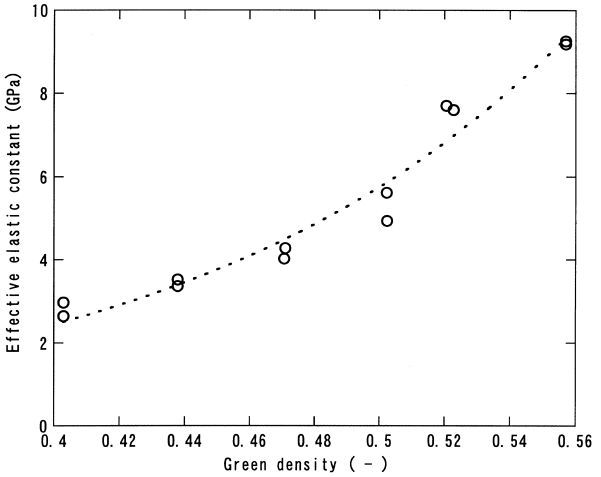

Fig. 6. Effective elastic constant of UO_2 powder.

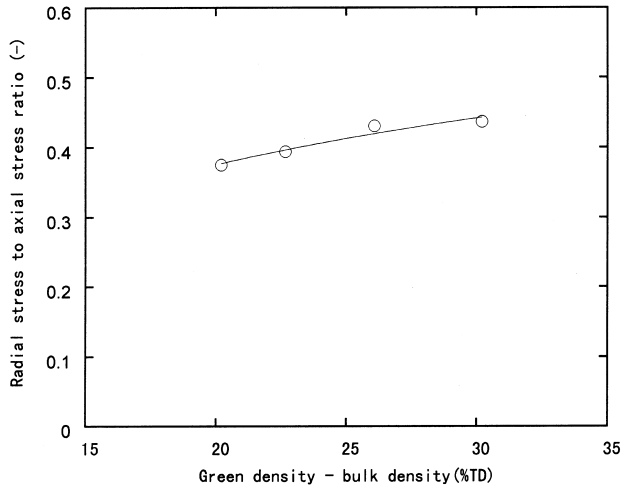

Fig. 7. Radial stress to axial stress ratio during uniaxial dry press of powder.

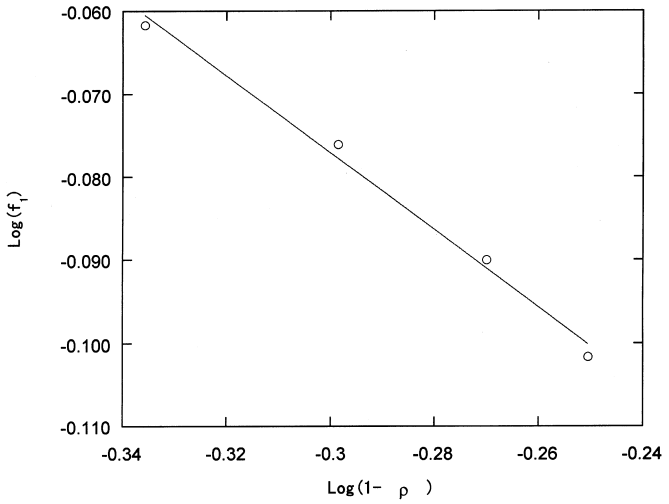

Fig. 8. Green density dependence of parameter f_1.

friction coefficient can be obtained experimentally by measurements of the radial stress to axial stress ratio (ξ) and friction force (σ_f) at σ_z.

Fig. 11 shows the experimental results of friction coefficient of UO_2 powder and die surface made of tungsten carbide. From this figure, the friction coefficient between the UO_2 powder and die surface has hardly any dependence on compaction pressure during the double acting dry press process. In this study, the friction coefficient was assumed to be constant during the compaction process, and the averaged value of the measured friction coefficient (0.181) was used for the boundary condition at the lateral surface of the green pellet in the analysis by FEM.

5. Results and discussion of FEM analysis

5.1. Convergence of calculation results of density distribution

Fig. 12 represents the calculated density distribution of UO_2 green pellet for the conditions shown in Table 2. In analysis of the density distribution in the green pellet fabricated by the double acting dry press, nodal points near the lateral portion are configured with a smaller interval than that of the central portion to simulate a larger density fluctuation for the lateral portion (Fig. 4). From Fig. 12, the green pellet fabricated by the double acting dry press has a large density fluctuation near the

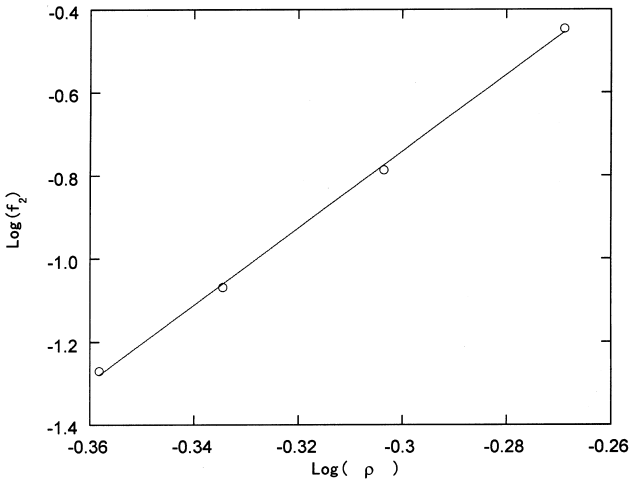

Fig. 9. Green density dependence of parameter f_2.

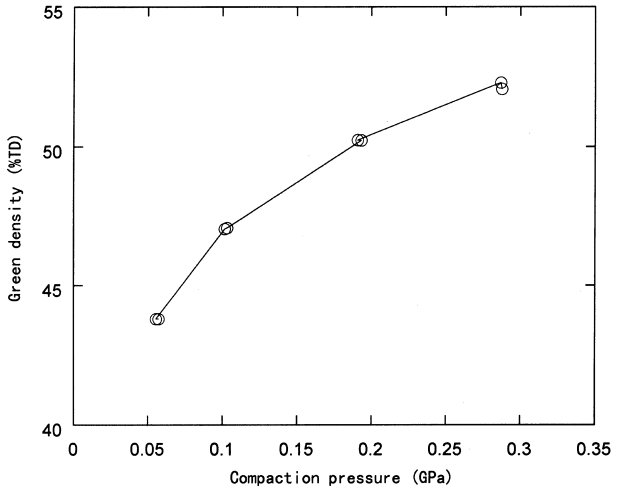

Fig. 10. Compaction pressure dependence of green density.

lateral surface. This fluctuation is considered to be generated by the friction force between the UO_2 powder and die surface during powder compaction. In the first quadrant, this friction force obstructs the downward powder flow at the die surface, and axial stress cannot be completely transmitted to the center portion at the lateral surface of the green pellet, so the maximum density fluctuation occurs along this lateral surface. In this study, this density distribution along the lateral surface is used for the confirmation of calculation convergence.

Calculations by the FEM code are generally time consuming and the calculation time is directly dependent on step width and division number of finite elements. In order to confirm calculation convergence, dependencies for step width and the number of elements of the

Table 1
Elastic-plastic properties of UO_2 powder fabricated by ADU route

k_1	k_2	ρ_b	σ_{eq}	A	m	n
0.8957	3.6968	0.2363	105.3 GPa	1.644	0.4387	9.251

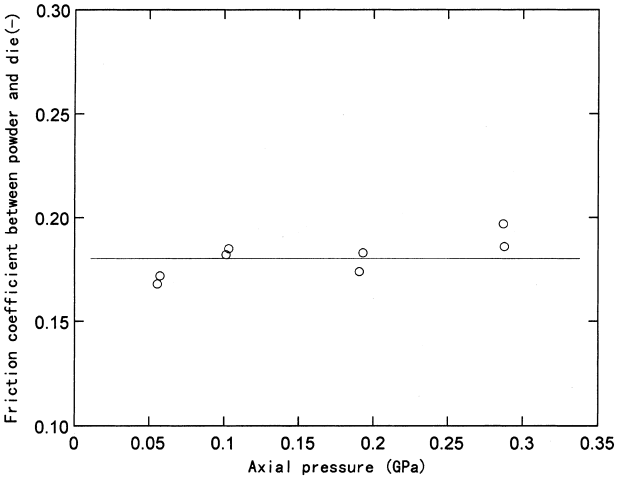

Fig. 11. Friction coefficient between powder and die surface.

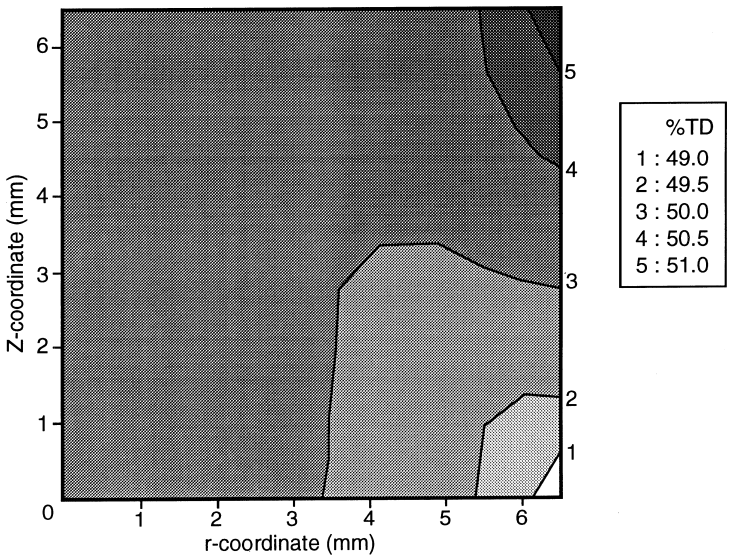

Fig. 12. Density distribution in UO_2 green pellet calculated by FEM code (flat pellet).

calculated results were tested. Fig. 13 represents the step width dependence of the density distribution along the lateral position ($r/r_0 = 0.985$) of the green pellet. Sufficient convergence can be obtained for the step width range smaller than the step width corresponding to 0.4% TD of the relative density increase. Fig. 14 shows the dependence for the division number of elements dependence of density distribution along the lateral portion ($r/r_0 = 0.985$) of the green pellet. From this figure, the local density calculated by this FEM code does not change beyond 0.3% TD, even if the number of elements was changed when the first quadrant of the green pellet was divided by more than five elements along both axial and radial directions.

Table 2
Calculation conditions for density distribution analysis

Initial density	Diameter	L/D ratio (after compaction)	Compaction pressure	Friction coefficient	Step width	Number of elements
30% TD	13 mm	1	200 MPa	0.181	0.1% TD	7×7

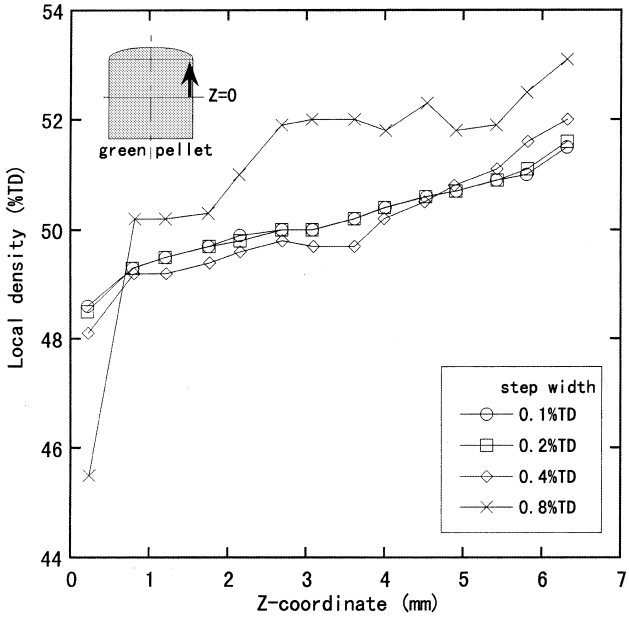

Fig. 13. Axial density distribution in UO_2 green pellet (calculation step width dependence, $r/r_0 = 0.985$).

From the above results, the convergence of this FEM code is confirmed for practical calculation conditions.

5.2. Comparison with experiments

Fig. 15 represents yield locus for UO_2 powder evaluated by Eq. (5) together with pressure dependence of green density fabricated by cold static press and double acting dry press. The data for double acting dry press were plotted along the dotted line which was drawn using experimental results shown in Fig. 7. From this figure, the yield function used in this study is considered to express the compaction behavior of UO_2 powder precisely in the wide range of green density.

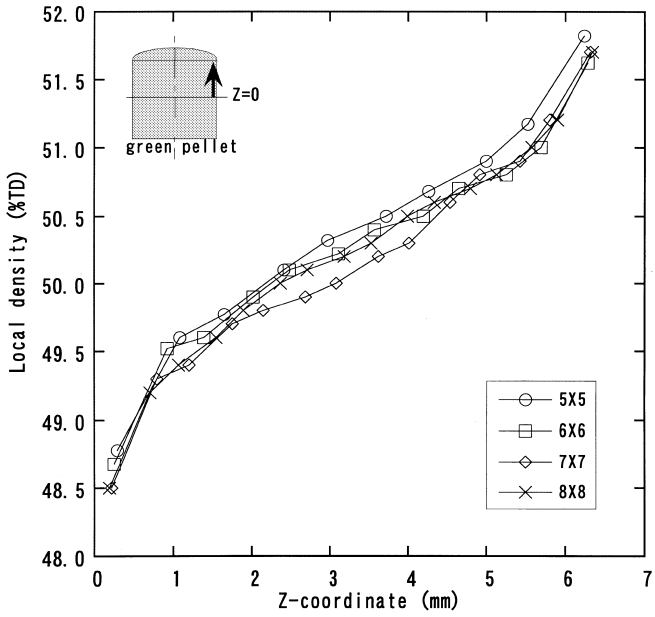

Fig. 14. Axial density distribution in UO_2 green pellet (number of elements dependence, $r/r_0 = 0.985$).

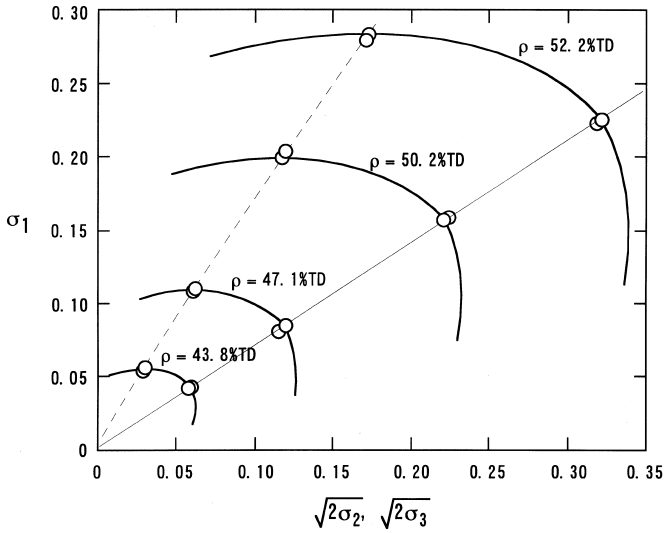

Fig. 15. Comparison of yield locus evaluated by Eq. (5) and green density fabricated by cold isostatic press and double acting dry press.

The local density in the UO_2 green pellet can be measured by using energy dispersive X-ray analysis (EDX) [5]. Calculation results are compared with the EDX experimental results shown in Fig. 16. In this comparison, compaction conditions and UO_2 powder used were the same for both EDX and FEM. The EDX measured data show that the local density at the corner portion in the green pellet fabricated by the double acting dry press is very high and the inner portion has a relatively homogeneous density distribution. The local density at the center portion has a slightly higher value than that at the intermediate portion. All of these tendencies are well simulated by the calculation by the FEM code developed. The difference in local densities estimated by the calculation and the experiment is less than 0.5% TD.

Fig. 17 shows pellet length to diameter ratio (L/D ratio) dependence of averaged green density evaluated by FEM calculation and measurement of dimension and

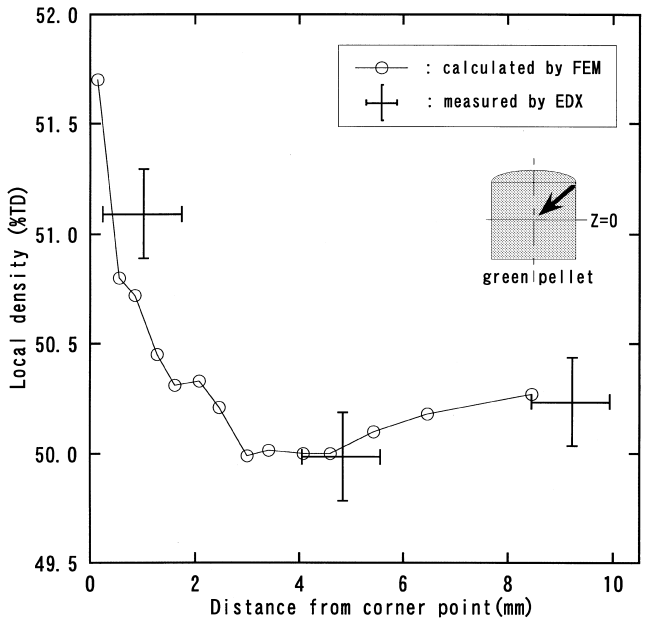

Fig. 16. Comparison of local densities estimated by FEM and EDX.

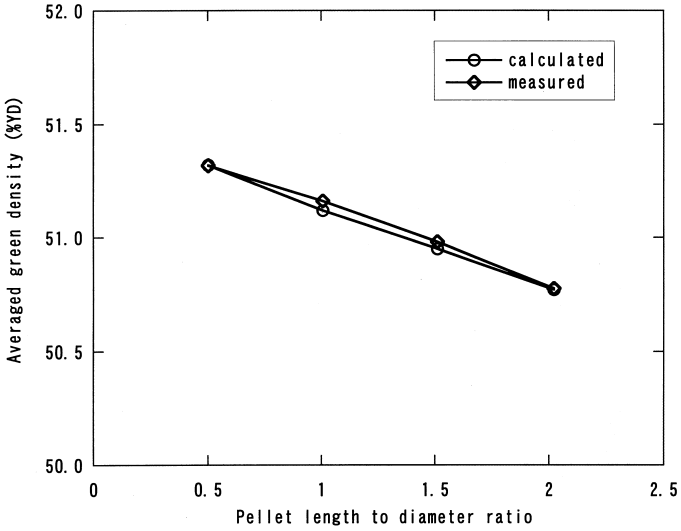

Fig. 17. Pellet length to diameter ratio dependence of averaged green density.

weight of UO_2 green pellet. In the double action dry press process, the die friction force acting on the surface of the green pellet during compaction increases with the increase of the L/D ratio of the green pellet. In the case of larger L/D ratio of the green pellet, the density distribution in the green pellet becomes more heterogeneous which results in the decrease of the averaged green density. As shown in Fig. 17, the averaged green density obtained by the measurements decreases with the increase of L/D ratio of the green pellet, and this L/D ratio dependence of the green density is well simulated by the FEM code.

From these results, it is judged this FEM code can be used for the quantitative estimation of the density distribution or stress distribution in the UO_2 green pellet during compaction. And this FEM code can be applied to other ceramic powdered material whose materials properties can be described by the same elastic–plastic model in which material constants can be determined by experimental measurements.

5.3. Parametric study

5.3.1. Compaction pressure

Fig. 18 shows compaction pressure dependence of the axial density distribution in the UO_2 green pellet. The local density fluctuation in the green pellet has hardly any dependence upon the compaction pressure in the range of the calculation conditions. From Fig. 10, the effect of compaction pressure on the green density decreases with the increase of the compaction pressure. The above calculation results of compaction pressure dependence are interpreted as results for the increase of stress heterogeneity in the green pellet at higher compaction pressure. This is considered to be caused by deterioration of the rearrangement ability of powder particles in the green pellet at the higher compaction pressure.

5.3.2. Pellet length to diameter ratio

Fig. 19 shows the axial density distribution of green pellets which have length to diameter ratios (L/D ratio) of 0.5, 1.0, and 2.0. The local density at the center portion of the lateral surface in the green pellet decreases with the increase of L/D ratio. This tendency is caused by the friction force at the die surface which obstructs the powder flow toward the center portion of the green pellet and transmission of the compressive stress from the surfaces of upper and lower punches to the inner portion of the green pellet. This result agrees with the experimental result of bottom-to-top ram pressure ratio for Cu compact [24]. From the results of L/D ratio dependence, it is considered that the density heterogeneity in the green pellet grows more serious and hourglassing of the as-sintered pellet increases with the increase of L/D ratio of the green pellet.

6. Conclusions

1. The FEM code which can be used to analyze stresses and density distribution in the ceramic green pellet during powder compaction was developed using an elastic–plastic model.
2. The experimental results of local density in UO_2 green pellet which was compacted by the double acting dry press process were well simulated by the results calculated in the above code.
3. For calculation in the above FEM code, the density fluctuation in the green pellet fabricated by

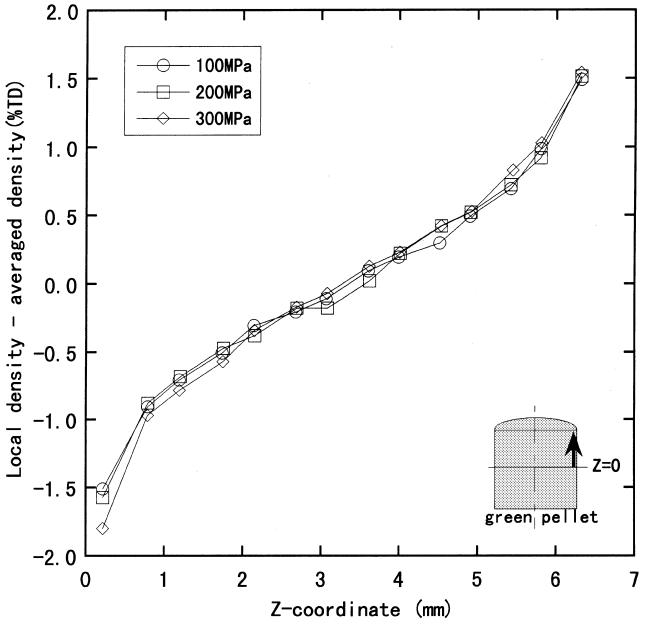

Fig. 18. Axial density distribution in UO_2 green pellet (compaction pressure dependence, $r/r_0 = 0.985$).

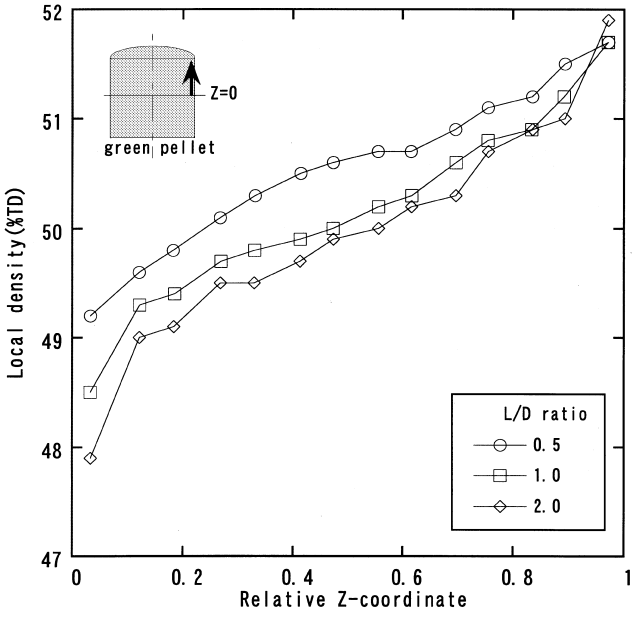

Fig. 19. Axial density distribution in UO_2 green pellet (length to diameter ratio dependence, $r/r_0 = 0.985$).

double acting dry pressing increased with the increase of pellet length to diameter ratio. The axial density fluctuation at the lateral portion in the UO_2 green pellet was hardly dependent upon compaction pressure.

Acknowledgements

The authors would like to thank Professor H.Furuya at Kyushu University and Dr K. Ito of Hitachi Ltd. for their valuable comments regarding this work.

References

[1] R.A. Thompson, Ceram. Bull. 60 (2) (1981) 244.
[2] P.V. Marshall, P. York, J.Q. Maclaine, Powder Technol. 74 (2) (1993) 171.
[3] W.D. Kingery et al., Introduction to Ceramics, Wiley, New York, 1976.
[4] D. Olander, Fundamental Aspects of Nuclear Reactor Fuel Elements, TID26711-P1, 1976, p. 580.
[5] K. Yanai, S. Ishimoto, T. Kubo, K. Ito, T. Ishikawa, H. Hayashi, J. Nucl. Mater. 224 (1995) 79.
[6] D. Train, Trans. Inst. Chem. Eng. 35 (1957) 258.
[7] G.C. Kuczynski, I. Zaplatynskij, J. Metals 206 (1956) 215.
[8] O. Abe, S. Iwai, S. Kanzaki, M. Ohashi, H. Tabata, Yogyo-Kyokai-Shi 94 (10) (1986) 1092.
[9] P.A. Cundall, C.D.L. Strack, Geotechnique 29 (1) (1979) 47.
[10] T. Nakagawa, M. Sato, in: Proc. 1992 Powd. Metallur. Cong., 1992, p. 43.
[11] P. Mosbah, D. Bouvard, in: Proc. 1996 Powd. Metallur. Cong., 1996, p. 7.
[12] D.T. Gethin, R.W. Lewis, D.V. Tran, A.K. Ariffin, in: Proc. 1994 Powd. Metallur. Cong., 1994, p. 13.
[13] J. Yoshida, in: Proc. Fifteenth Doboku Joho System Symposium, 1990, p. 35.
[14] S. Shima, G. Sugiyama, J. Lian, in: Proc. 1993 Powd. Metallur. Cong., 1993, p. 327.
[15] S. Tamura, T. Aizawa, J. Kihara, in: Proc. 1993 Powd. Metallur. Cong., 1993, p. 323.
[16] S. Tamura, PhD thesis, Tokyo Univ., 1995.
[17] S. Shima, Summary of Spring Meeting of Japan Soc. Powd. and Powd. Metallur., 1994, p. 40.
[18] Y. Taguchi, in: Proc. Spring Ordinary Meeting of Soc. Powd. Technol. Japan, 1993, p. 98.
[19] O.C. Zienkiewicz, The Finite Element Method, McGraw-Hill, Maidenhead, UK, 1977.
[20] S. Shima, N. Hirata, T. Hirao, M.A. Saleh, in: Proc. Sosei-kako-shunki-kouenkai, 1989, p. 211.
[21] N. Igata, K. Domoto, J. Nucl. Mater. 45 (1972/1973) 317.
[22] S. Shima, M. Oyane, Int. J. Mech. Sci. 18 (6) (1976) 285.
[23] K. Okimoto, M. Oyane, S. Shima, Kyushu-Kogyo-Gijutushikenjo-Hokoku 29 (1982) 1892.
[24] R.A. Thompson, Ceram. Bull. 60 (2) (1981) 237.